CHALMERS
UNIVERSITY OF TECHNOLOGY

Model-Driven End-to-End Learning for Integrated Sensing and Communication

Model-Driven End-to-End Learning for Integrated Sensing and Communication

José Miguel Mateos-Ramos*, Christian Häger*,
Musa Furkan Keskin*, Luc Le Magoarou†, Henk Wymeersch*
*Department of Electrical Engineering, Chalmers University of Technology, Sweden
†Univ Rennes, INSA Rennes, CNRS, IETR-UMR 6164, Rennes, France

***Abstract*—Integrated sensing and communication (ISAC) is envisioned to be one of the pillars of 6G. However, 6G is also expected to be severely affected by hardware impairments. Under such impairments, standard model-based approaches might fail if they do not capture the underlying reality. To this end, data-driven methods are an alternative to deal with cases where imperfections cannot be easily modeled. In this paper, we propose a model-driven learning architecture for joint single-target multi-input multi-output (MIMO) sensing and multi-input single-output (MISO) communication. We compare it with a standard neural network approach under complexity constraints. Results show that under hardware impairments, both learning methods yield better results than the model-based standard baseline. If complexity constraints are further introduced, model-driven learning outperforms the neural-network-based approach. Model-driven learning also shows better generalization performance for new unseen testing scenarios.**

***Index Terms*—Auto-encoder, integrated sensing and communication, joint radar and communications, model-driven machine learning.**

I. Introduction

Integrated sensing and communication (ISAC) has in the past few years become one of the key enabling technologies within the vision for 6G [1]–[3]. In this 6G context, ISAC not only provides a means to reuse communication infrastructure for sensing purposes, it also provides a way to optimize the operation of the communication system itself, in the form of blockage prediction, radio mapping, and proactive resource allocation.

ISAC can be broadly categorized as *radar-centric* and *communication-centric*. In radar-centric design, the aim is to provide communication capabilities on top of existing radar sensing infrastructure, as e.g., in [4], [5]. Generally, radar-centric designs exhibit poor communication performance, driven largely by hardware and cost constraints. Communication-centric ISAC relies on modifying communication waveforms and signal processing to enable high-resolution sensing. At a cost of a potential reduction in data rate, flexible sensing performance is attained, due to the high degree of freedom provided in communication signal optimization, including power allocation, beamforming design, and scheduling [6], [7].

This work was supported, in part, by a grant from the Chalmers AI Research Center Consortium (CHAIR), by the European Commission through the H2020 project Hexa-X (Grant Agreement no. 101015956) and by the MSCA-IF grant 888913 (OTFS-RADCOM). The work of C. Häger was also supported by the Swedish Research Council under grant no. 2020-04718.

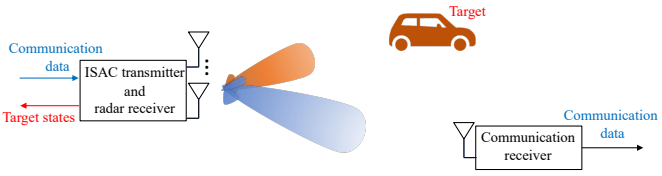

Fig. 1: Considered ISAC scenario with an ISAC transmitter, co-located sensing/radar receiver, and a remote communication receiver. The learned transmit beams provide a flexible trade-off between sensing and communication.

Within communication-centric ISAC, both the problem of signal design and that of signal processing have been traditionally treated under the umbrella of model-based signal processing. Model-based methods have important benefits, such as performance guarantees, explainability, and predictable computational complexity. However, they suffer from performance degradation under model mismatch and can be hard to derive when models are complicated. These issues have been addressed via data-driven designs, relying on machine learning (ML). Among ML-based ISAC works, we mention [8]–[15]. In [8], the potential of ML in ISAC is discussed. An extensive survey on ML in ISAC is provided in [9], though with an emphasis on sensing. In [10], ML is used in sensing to learn the model order. In [11], a two-level multi-task artificial neural network is proposed to replace the ISAC receiver, which is shown to mitigate the imperfections and non-linearities of THz systems. In [12], ML-aided beamforming in ISAC is tackled, where a neural network learns the mapping from received signal to angle (see also [16]). A vehicular beamforming scenario is considered in [13], [14], where ML is applied to learn beamformers. Finally, in our previous work [15], we developed an end-to-end approach for the ISAC problem, applying an autoencoder (AE) [17] to account for hardware impairments. These ML-based approaches to ISAC can operate under model mismatch and in general require little knowledge about the problem, other than the loss function. The drawbacks of this class of methods lies in the lack of performance guarantees, limited interpretability, and often high training complexity.

A third way, in between model-based and ML-based ISAC is provided by so-called *model-driven ML (MD-ML)* [18]. This recent approach proved particularly relevant for communication systems [19], [20], due to the abundance of models characterizing them. In MD-ML, existing designs, algorithms or functional decompositions are reformulated as structured neural networks. An early example is the principle of deep

unfolding [21], [22], in which the iterations of an iterative method are interpreted as the layers of a neural network (see [23] for a survey of deep unfolding applied to communication systems). As an added benefit, the neural network can be initialized from the model-based counterpart, thus starting from a already reasonably well performing point instead of at random. Especially relevant for ISAC are models linking sent or received signal at antenna arrays to directions of propagation. For instance, in [24], the steering vector models are taken as an initialization and made flexible by learning with a neural network of varying depth unfolding the matching pursuit algorithm [25]. The approach was then optimized and extended to the frequency response vector model in [26].

In this paper, we apply MD-ML for end-to-end ISAC. Although MD-ML has been investigated in communication scenarios [19], [20], [23], [24], [26], there is no research on MD-ML for sensing. Our main contribution is to apply MD-ML to single-target sensing and extend this approach to obtain performance trade-offs between sensing and a MISO communication link. As MD-ML end-to-end learning, we optimize a model-based matrix of steering vectors to account for hardware impairments. However, unlike [24], we propose an architecture with parameter sharing to perform 2 tasks simultaneously: (i) precoder designing at the transmitter and (ii) target angle-of-arrival (AoA) estimation at the receiver. A comparison between (i) MD-ML, (ii) neural-network-based learning and (iii) the best-known baseline is made under hardware impairments and complexity constraints.

II. System Model

In this section, we describe the considered ISAC scenario, which is depicted in Fig. 1.

A. Sensing Model

We consider a monostatic radar with a uniform linear array (ULA) of K antenna elements. At each transmission, the transmitter sends a complex signal $\boldsymbol{x} \in \mathbb{C}^K$, subject to $\mathbb{E}[\|\boldsymbol{x}\|^2] \leq E_{\text{tx}}$. A single target in the environment might reflect the signal back to the transmitter. The probability that the target is present is drawn from a Bernoulli distribution $t \sim \text{Bern}(1/2)$. If a target is present ($t = 1$), the received signal at the ULA is

$$\boldsymbol{y}_r = \alpha \boldsymbol{a}_{\text{rx}}(\theta)\boldsymbol{a}_{\text{tx}}^\top(\theta)\boldsymbol{x} + \boldsymbol{n}, \tag{1}$$

where we assume a Swerling-1 model of the target, such that $\alpha \sim \mathcal{CN}(0, \sigma_r^2)$, with σ_r^2 representing the loss of power due to path loss and the target's radar cross section. The steering vector is $[\boldsymbol{a}_{\text{tx}}(\theta)]_k = [\boldsymbol{a}_{\text{rx}}(\theta)]_k = \exp(-\jmath 2\pi(k - (K-1)/2)d\sin(\theta)/\lambda)$, with $d = \lambda/2$ and λ the wavelength. The AoA of the target θ, is uniformly distributed as $\theta \sim \mathcal{U}[\theta_{\min}, \theta_{\max}]$. The prior knowledge $\{\theta_{\min}, \theta_{\max}\}$ is assumed to be available, with $-\pi/2 \leq \theta_{\min} \leq \theta_{\max} \leq \pi/2$. Regardless of the target presence, complex Gaussian noise $\boldsymbol{n} \sim \mathcal{CN}(\boldsymbol{0}, N_0\boldsymbol{I}_K)$ is added at the receiver side.

The goal of the co-located receiver is to maximize the detection probability of the target, subject to some false alarm probability, and to estimate θ in the case of target detection, based on $\boldsymbol{y}_r$.

B. Communication Model

We consider the same transmitter of K antenna elements. The transmitter maps a message $m \in \mathcal{M}$ from a set of possible messages $\mathcal{M}$ into a complex symbol $s(m) \in \mathbb{C}$. The symbol $s(m)$ is precoded by $\boldsymbol{v} \in \mathbb{C}^K$ to steer the ULA energy towards the receiver direction. The output signal is $\boldsymbol{x}(m) = \boldsymbol{v}s(m)$, again subject to $\mathbb{E}[\|\boldsymbol{x}\|^2] \leq E_{\text{tx}}$. The receiver has a single antenna element, which yields a MISO communication link. The communication receiver is always present, and the received signal follows the model

$$y_c = \beta \boldsymbol{a}_{\text{tx}}^\top(\vartheta)\boldsymbol{x}(m) + n, \tag{2}$$

where a Rayleigh channel is considered, with $\beta \sim \mathcal{CN}(0, \sigma_c^2)$ and $n \sim \mathcal{CN}(0, N_0)$, and the communication receiver is randomly located in a certain angle-of-departure (AoD) range $\vartheta \sim \mathcal{U}[\vartheta_{\min}, \vartheta_{\max}]$, with prior knowledge of $\{\vartheta_{\min}, \vartheta_{\max}\}$ and $-\pi/2 \leq \vartheta_{\min} \leq \vartheta_{\max} \leq \pi/2$. We also assume that the receiver has access to the channel state information (CSI) $\kappa = \beta \boldsymbol{a}_{\text{tx}}^\top(\vartheta)\boldsymbol{v}$ through a pilot sequence transmission.

The goal of the remote receiver is to retrieve the transmitted message based on the observation y_c.

C. Integrated Sensing and Communication

The purpose of ISAC is to combine the sensing and communication transmitters into a joint transmitter that can be optimized to allocate energy between the target and the communication receiver direction. The transmitter considers the joint a priori angular information $\boldsymbol{\Theta} = \{\theta_{\min}, \theta_{\max}, \vartheta_{\min}, \vartheta_{\max}\}$. The receivers and the transmitter can be jointly optimized to obtain a trade-off between communication and sensing performance.

III. Baseline Approach

The proposed learning approach is highly driven by the structure of standard model-based methods. Here we provide the derivation of the baseline, which is compared later with end-to-end learning approaches in Section V.

A. Transmitter Benchmark

We design the benchmark for the transmit beamformer $\boldsymbol{x}$ in (1) or (2) by resorting to the beampattern synthesis approach in [27], [28]. We define a uniform angular grid covering $[-\pi/2, \pi/2]$ with N_{grid} grid locations $\{\theta_i\}_{i=1}^{N_{\text{grid}}}$. For a given angular range $\boldsymbol{\theta}_{\text{range}}$, we denote by $\boldsymbol{b} \in \mathbb{C}^{N_{\text{grid}} \times 1}$ the desired beampattern over the defined angular grid, given by

$$[\boldsymbol{b}]_i = \begin{cases} K, & \text{if } \theta_i \in \boldsymbol{\theta}_{\text{range}} \\ 0, & \text{otherwise.} \end{cases} \tag{3}$$

The problem of beampattern synthesis can then be formulated as $\min_{\boldsymbol{x}} \left\|\boldsymbol{b} - \boldsymbol{A}^\top\boldsymbol{x}\right\|_2^2$, where $\boldsymbol{A} = \left[\boldsymbol{a}_{\text{tx}}(\theta_1) \ \dots \ \boldsymbol{a}_{\text{tx}}(\theta_{N_{\text{grid}}})\right] \in \mathbb{C}^{K \times N_{\text{grid}}}$ denotes the transmit steering matrix evaluated at the grid locations. This least-squares (LS) problem has a simple closed-form solution

$$\boldsymbol{x} = (\boldsymbol{A}^*\boldsymbol{A}^\top)^{-1}\boldsymbol{A}^*\boldsymbol{b}, \tag{4}$$

which yields, after normalization according to the transmit power constraints, a communication-optimal beam $\boldsymbol{x}_c$ or a radar-optimal beam $\boldsymbol{x}_r$.

For ISAC scenarios, a radar-communication trade-off beam is needed to provide adjustable trade-offs between the two functionalities. Using the approach from [29], we design the ISAC beam as

$$\boldsymbol{v}(\rho,\varphi) = \sqrt{E_{\text{tx}}}\frac{\sqrt{\rho}\boldsymbol{x}_r + \sqrt{1-\rho}e^{\jmath\varphi}\boldsymbol{x}_c}{\|\sqrt{\rho}\boldsymbol{x}_r + \sqrt{1-\rho}e^{\jmath\varphi}\boldsymbol{x}_c\|}\ , \tag{5}$$

where $\rho \in [0,1]$ is the ISAC trade-off parameter and $\varphi \in [0, 2\pi)$ is a phase ensuring coherency between multiple beams. By sweeping over ρ, we explore the ISAC performance of the baseline.

B. Radar Detection Benchmark

Since the radar detection problem in (1) involves random parameters α and θ, we derive the maximum a-posteriori (MAP) ratio test (MAPRT) detector [30] as our detector benchmark, which takes into account the prior information on α and θ. Let $\mathcal{H}_0$ and $\mathcal{H}_1$ denote the absence and the presence of a target, respectively, in (1). Then, the corresponding MAPRT is given by [30]

$$\mathcal{L}(\boldsymbol{y}_r) = \frac{\max_{\alpha,\theta,\boldsymbol{x}} p(\alpha,\theta,\boldsymbol{x},\mathcal{H}_1 \,|\, \boldsymbol{y}_r)}{p(\mathcal{H}_0 \,|\, \boldsymbol{y}_r)} \underset{\mathcal{H}_0}{\overset{\mathcal{H}_1}{\gtrless}} \widetilde{\eta}\ . \tag{6}$$

Assuming $p(\mathcal{H}_0) = p(\mathcal{H}_1) = 1/2$, we find, after some derivation, that the test simplifies to[1](see [15, App. A])

$$\left|\boldsymbol{a}_{\text{rx}}^{\mathsf{H}}(\widehat{\theta})\boldsymbol{y}_r\right|^2 \underset{\mathcal{H}_0}{\overset{\mathcal{H}_1}{\gtrless}} \overline{\eta}\ , \tag{7}$$

where $\overline{\eta}$ is a threshold determined based on a given false alarm probability and

$$\widehat{\theta} = \arg \max_{\theta\in[\theta_{\min},\theta_{\max}]} \left|\boldsymbol{a}_{\text{rx}}^{\mathsf{H}}(\theta)\boldsymbol{y}_r\right|^2\ . \tag{8}$$

C. Communication Receiver Benchmark

Given the CSI $\kappa = \beta\boldsymbol{a}_{\text{rx}}^{\top}(\theta)\boldsymbol{v}$, the received signal is $y_c = \kappa s(m) + n$. Hence, symbol error rate (SER) is minimized by using maximum likelihood estimation (MLE) as $\hat{m}(y_c) = \arg\min_{m\in\mathcal{M}} \|y_c - \kappa s(m)\|^2$.

IV. ISAC end-to-end Learning

In the following, we first describe the architecture of neural-network-based learning and the loss functions involved during training for the ISAC scenario. Then, we specify how model-driven learning is trained, and how the ISAC trade-offs are assessed. In Fig. 2 we represent how the different components of the system are related for model-driven learning.

A. Neural-Network-Based End-to-End Learning

We use 5 feed-forward neural networks as depicted in Table I. This AE architecture is based on our previous work [15], with some modifications. On the transmitter side, the encoder takes a one-hot encoded message m and outputs a complex number interpreted as the symbol of a constellation. The beamformer uses as input the prior information $\boldsymbol{\Theta}$ to yield a complex precoder $\boldsymbol{v}$. The radar receiver is divided into 2 networks: (i) for target detection, the network concatenates the received signal $\boldsymbol{y}_r$ and the sensing angular information $\{\theta_{\min}, \theta_{\max}\}$ as input, to predict the target probability as output; (ii) the angle estimator uses the same input as the presence detector, but it gives an estimate of the target angle $\widehat{\theta}$. The communication receiver maps the concatenation of the received signal y_c and the CSI κ to a vector of probabilities $\hat{\boldsymbol{m}}$, where the i-th element of $\hat{\boldsymbol{m}}$ represents the probability that the i-th message was transmitted. For complex-valued inputs or outputs, the concatenation of the real and imaginary parts is utilized. In Table I, the dimensions correspond to the real-valued concatenated vectors.

TABLE I: Neural network architectures.

Network	Input layer	Hidden layers	Output layer
Encoder $f_{\boldsymbol{\varepsilon}}$	$\lvert\mathcal{M}\rvert$	$(K, K, 2K)$	2 (linear)
Beamformer $f_{\boldsymbol{\mu}}$	4	(N, N, N)	$2K$ (linear)
Presence det. $f_{\boldsymbol{\rho}}$	$2K+2$	(N, N, N)	1 (sigmoid)
Angle est. $f_{\boldsymbol{\nu}}$	$2K+2$	(N, N, N)	1 (tanh)
Comm. receiver $f_{\boldsymbol{\eta}}$	4	$(K, 2K, 2K)$	$\lvert\mathcal{M}\rvert$ (softmax)

1) Loss Functions: We choose a suitable loss function based on the task to be solved.

- **Target Detection.** We use the binary cross-entropy (BCE) loss. Let $\hat{p} \in [0,1]$ be the estimate of the probability that the target is in the environment. The BCE loss is then
$$\mathcal{J}_{\text{TD}} = -\mathbb{E}[t\log(\hat{p}) + (1-t)\log(1-\hat{p})]. \tag{9}$$
- **Angle Estimation.** We use the mean squared error (MSE) loss between the estimated and true angles according to $\mathcal{J}_{\text{angle}} = \mathbb{E}[|\hat{\theta} - \theta|^2]$. Note that this loss is meaningful only when $t = 1$ and the neural network estimates that there is a target.
- **Communication Message Estimation.** We treat this problem as a multi-class classification problem, where each of the classes corresponds to a transmitted message. Hence, we resort to the categorical cross-entropy (CCE) loss. Let $\boldsymbol{m}^{\text{enc}} \in \{0,1\}^{|\mathcal{M}|}$ be the one-hot encoding of m and $\hat{\boldsymbol{m}} \in [0,1]^{|\mathcal{M}|}$ a $|\mathcal{M}|$-dimensional probability vector. Then, the CCE loss is
$$\mathcal{J}_{\text{comm}} = -\mathbb{E}\left[\sum_{j=1}^{|\mathcal{M}|} m_j^{\text{enc}}\log(\hat{m}_j)\right]. \tag{10}$$

2) Neural-network Based ISAC: To obtain a good ISAC trade-off, we could train all 5 networks from Table I at the same time. However, the scale of the detection and angle estimation loss functions might differ in several orders of magnitude. Then, we apply a 2-step learning procedure. Firstly, we learn $\boldsymbol{\varepsilon}, \boldsymbol{\mu}, \boldsymbol{\rho}, \boldsymbol{\eta}$ based on target detection using the following loss function

$$\mathcal{J}_{\text{ISAC}}^{\text{TD}} = \omega_r \mathbb{I}\{t=1\}\mathcal{J}_{\text{TD}} + (1-\omega_r)\mathcal{J}_{\text{comm}}, \tag{11}$$

where $\omega_r \in [0,1]$ is a hyperparameter that allows for flexible trade-offs between sensing and communication performance,

[1]Although $\boldsymbol{x}$ is known to the radar receiver, taking it as unknown in the MAPRT formulation (6) and plugging in its optimal value as a function of θ simplify the detection test in [15, Eq. (16)] to a simple matched filter receiver in (7).

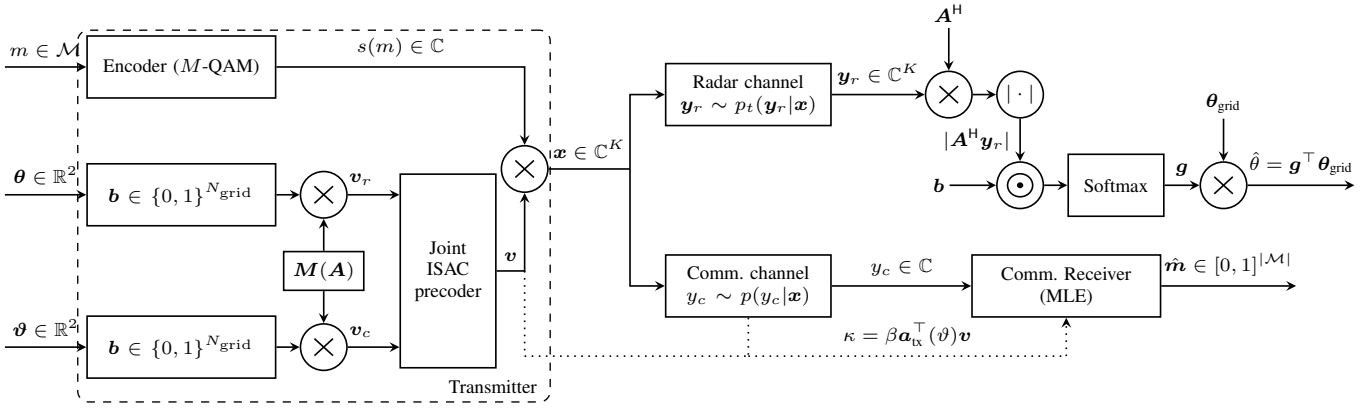

Fig. 2: Block diagram of the ISAC model-driven approach. The matrix $\boldsymbol{A} \in \mathbb{C}^{K \times N_{\text{grid}}}$ is optimized via end-to-end learning by only considering single-target sensing. The communication encoder and receiver are implemented as in the baseline with no learnable parameters.

and $\mathbb{I}\{\cdot\}$ is the indicator function. Secondly, we learn $\boldsymbol{\nu}$ and update $\boldsymbol{\varepsilon}, \boldsymbol{\mu}, \boldsymbol{\eta}$ by training for angle estimation, using the joint loss function

$$\mathcal{J}_{\text{ISAC}}^{\text{angle}} = \omega_r \mathcal{J}_{\text{angle}} + (1-\omega_r)\mathcal{J}_{\text{comm}}. \tag{12}$$

B. Model-Driven end-to-end Learning

1) Trainable Model-Driven Transmitter: According to the benchmark, the transmitter precoder is based on (4), which involves the vector $\boldsymbol{b}$ and the matrix of steering vectors $\boldsymbol{A}$. The binary vector $\boldsymbol{b}$ is completely determined by the prior angular information $\boldsymbol{\theta}_{\text{range}}$. We let $\boldsymbol{A} \in \mathbb{C}^{K \times N_{\text{grid}}}$ be a matrix of complex trainable parameters. In this way, the matrix $\boldsymbol{A}$ is able to adapt to the hardware impairments in the transmitter ULA that are described in Section V-C.

Nevertheless, (4) involves a matrix inversion. Therefore, we instead compute a matrix $\boldsymbol{M}$, which is the result of the matrix equation $(\boldsymbol{A}^*\boldsymbol{A}^\top)\boldsymbol{M} = \boldsymbol{A}^*$. The transmitter signal is simply $\boldsymbol{x} = \boldsymbol{M}\boldsymbol{b}$, which is then normalized to have energy E_{tx}.

2) Trainable Model-Driven Sensing Receiver: The test statistic in (7) to compute the probability of detection is based on the angle estimation of the target. Hence, we imitate the same kind of procedure during learning, i.e., we only train $\boldsymbol{A}$ to yield a good angle estimate $\hat{\theta}$. Note that the same matrix $\boldsymbol{A}$ is shared between transmitter and receiver. Moreover, the angle estimation from the benchmark in (8) resorts to finding the argument that maximizes the test statistic. This operation is not differentiable, and we compute instead

$$\boldsymbol{g} = \text{softmax}(|\boldsymbol{A}^{\mathsf{H}}\boldsymbol{y}_r| \odot \boldsymbol{b}), \tag{13}$$

where we first compute the test statistic $|\boldsymbol{A}^H\boldsymbol{y}_r|$ similarly to the benchmark, but we restrict this metric to be within $\boldsymbol{\theta}_{\text{range}}$ by means of the element-wise product with $\boldsymbol{b}$. Ideally, $\boldsymbol{g}$ should be close to 1 in the position corresponding to the true angle. Hence, by computing $\boldsymbol{g}^\top\boldsymbol{\theta}_{\text{grid}}$, we expect to obtain a close estimation of the true angle.

Regarding target detection, even though we do not train the system for this task, we mimic (7) and perform detection based on

$$\max\{|\boldsymbol{A}^{\mathsf{H}}\boldsymbol{y}_r| \odot \boldsymbol{b}\} \underset{\mathcal{H}_0}{\overset{\mathcal{H}_1}{\gtrless}} \tilde{\eta}, \tag{14}$$

for some threshold $\tilde{\eta}$.

3) Model-based Communication Components: We use a standard $|\mathcal{M}|$-QAM encoder for the transmitter and the MLE approach from Section III-C at the receiver, which is optimal given the CSI. However, no parameters are trained for the communication link.

4) Model-driven ISAC: We note that, in contrast to neural-network-based learning, there is no need to directly train for ISAC, since the communication encoder and receiver are implemented following the baseline. Moreover, once we train $\boldsymbol{A}$ for sensing purposes, the transmitter can be used to point towards different directions (given different inputs). Hence, we train $\boldsymbol{A}$ solely for single-target sensing. After that, to evaluate the ISAC trade-offs, we create a joint precoder based on (5), with $\rho = \omega_r$ and $\varphi = 0$. In Fig. 2, it is depicted how we use different inputs to create a radar precoder ($\boldsymbol{v}_r$) and a communication precoder ($\boldsymbol{v}_r$), which are combined later following (5) to yield the ISAC precoder $\boldsymbol{v} \in \mathbb{C}^K$.

V. Results

In this section, we compare the performance of (i) model-driven learning, (ii) neural-network-based learning, and (iii) the model-based baseline described in Section III.

A. Parameter Selection, Random Training, and Evaluation

On the transmitter side, we consider an ULA with $K = 16$ antenna elements, $E_{\text{tx}} = 1$, and $|\mathcal{M}| = 4$ possible messages. The average radar signal-to-noise ratio (SNR) is chosen as $\text{SNR}_r = \sigma_r^2/N_0 = 0\,\text{dB}$ and the average communication SNR as $\text{SNR}_c = \sigma_c^2/N_0 = 20\,\text{dB}$.

For simplicity, we assume that the communication receiver is located at a random position within a fixed angular sector $[\vartheta_{\min}, \vartheta_{\max}] = [30°, 50°]$. However, in the sensing scenario, we randomize the angular sector of the target as in [31]. We first draw the mean angle of the sector as $\theta_{\text{mean}} \sim \mathcal{U}[-60°, 60°]$ and the span as $\Delta = \mathcal{U}[10°, 20°]$. The target prior information is then $\{\theta_{\min}, \theta_{\max}\} = \{\theta_{\text{mean}} - \Delta/2, \theta_{\text{mean}} + \Delta/2\}$. However, we show only results corresponding to a testing interval of $[\theta_{\min}, \theta_{\max}] = [-40°, -20°]$.

We use the Adam optimizer [32] for the learning approaches, with a learning rate of 10^{-3} and a batch size of

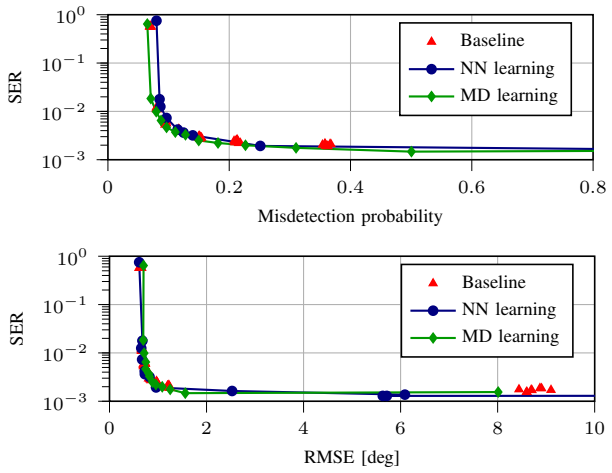

Fig. 3: Results without hardware impairments and without complexity restrictions. The target lies in the angular sector $[\theta_{\min}, \theta_{\max}] = [-40°, -20°]$.

10,000 samples. In model-driven learning, the matrix $\boldsymbol{A}$ is initialized as a perturbed version of the baseline steering matrix, i.e., $[\boldsymbol{A}]_{m,l} = \exp(-\jmath\pi(m-(K-1)/2)\sin(\theta_l)) + n$, with $n \sim \mathcal{N}(0, 0.1)$. The values for the trade-off parameter are $\omega_r \in \{0, 10^{-6}, 10^{-5}, 10^{-4}, 10^{-3}, 10^{-2}, 0.05, 0.1, 0.15, 0.4, 0.6, 0.8, 1\}$. For each ω_r value, we retrain all neural networks from scratch.

During the testing stage, we evaluate the performance of each method by computing the probability of misdetection $P_{\text{md}} = p(\hat{t} = 0 | t = 1)$, the SER $p(\hat{m} \neq m)$, and the sensing angle root mean squared error (RMSE) $\sqrt{E[|\hat{\theta} - \theta|^2]}$ for a given false alarm probability $P_{\text{fa}} = p(\hat{t} = 1 | t = 0) = 10^{-2}$. The RMSE is calculated only when the target is present and it has been detected by the receiver.

B. Results without Hardware Impairments

We first consider the case of ideal conditions in the ULA array ($d = \lambda/2$), without complexity restrictions. We set the number of hidden neurons in the neural networks of the sensing AE as $N = 1024$, giving approximately 6.4 million real-valued trainable parameters. We also fixed a grid of $N_{\text{grid}} = 500$ discrete angles, resulting in 8000 complex-valued trainable parameters for the model-driven learning architecture. Further increasing the number of parameters did not yield significant performance improvement. The number of training iterations is set to 50,000.

Fig. 3 shows the ISAC results for one particular testing angular sector. No significant differences can be observed between the learning approaches and the baseline. Indeed, for this scenario the baseline transmitter and receiver algorithms are either optimal (for communications) or close to optimal (for radar sensing). Moreover, without complexity constraints both learning approaches can be trained to perform similar to the baseline.

C. Results under Hardware Impairments

We now consider hardware impairments, which consist of perturbing the spacing between antenna elements in the transmitter ULA as $d_k \sim_{\text{i.i.d.}} \mathcal{N}(\lambda/2, \sigma_\lambda^2)$, with $k = 0, \ldots, K-2$. We assume $\sigma_\lambda = \lambda/30$. Fig. 4 shows the ISAC trade-off curves for a single realization of d_k. The main difference with respect to Fig. 3 is that the performance of the baseline drops in terms of angle estimation. This occurs naturally when the assumed models differ from reality (the assumed steering vector differs for hardware impairments). Conversely, when complexity is not limited, both end-to-end learning approaches are able to adapt to the impairments and show good performance, although neural-network learning slightly outperforms model-driven learning.

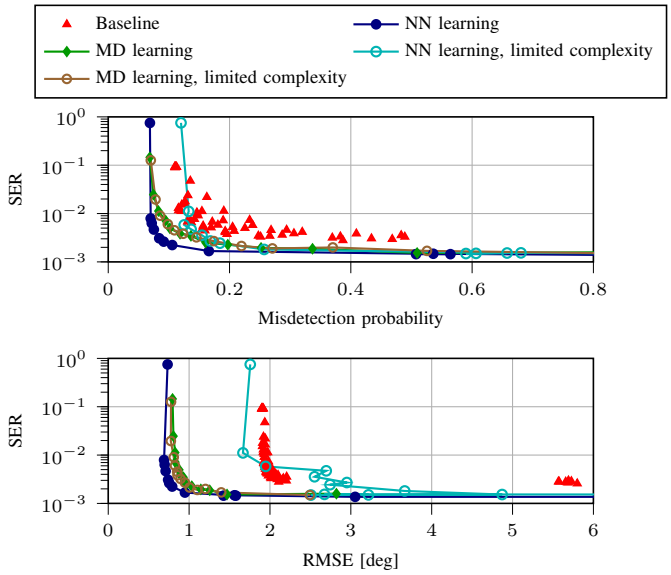

Fig. 4: Results under hardware impairments. The target lies in the angular sector $[\theta_{\min}, \theta_{\max}] = [-40°, -20°]$.

For complexity limitation, the number of hidden neurons in the neural-network-based learning is reduced to $N = 21$, and the grid points in $\boldsymbol{A}$ to $N_{\text{grid}} = 156$. This makes the number of trainable parameters of the sensing neural networks (approximately 5,000 real-valued parameters) comparable to the model-driven approach (approximately 2,500 complex-valued parameters). Neural-network-based degrades both for detection probability and angle estimation when the number of parameters is reduced. However, model-driven learning shows similar performance with respect to unlimited complexity. This indicates that in cases where complexity is limited, model-driven approaches perform better than neural-network-based learning.

D. Generalization Results

We now assess the generalization performance of the considered schemes via the testing scenario $[\theta_{\min}, \theta_{\max}] = [-20°, 20°]$ which is not included in the training dataset. Fig. 5 depicts the results assuming no complexity restrictions. We expected that the baseline would outperform learning approaches since they are tested on new unseen data. However, model-driven learning is the best approach, outperforming neural-network learning for both target detection and angle estimation. This implies that the model-driven approach does

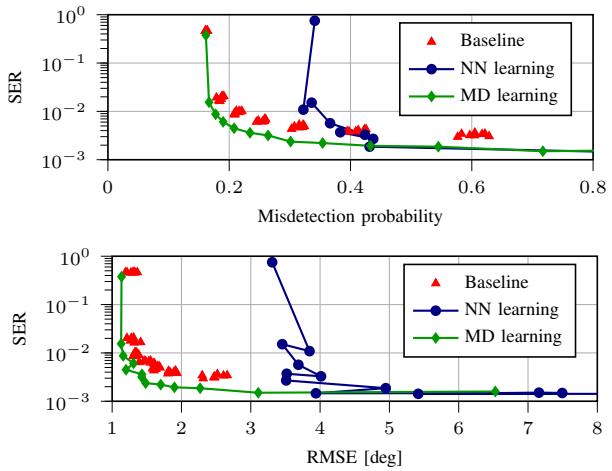

Fig. 5: Results under hardware impairments with low complexity constraints. The target lies in an angular sector $[\theta_{\min}, \theta_{\max}] = [-20°, 20°]$, which is not included in the training dataset.

not overfit to the training data, and it also captures the model structure of the impaired steering vectors.

VI. Conclusions

In this work, we have developed a model-driven ML approach for ISAC and compared to both a neural-network-based ML approach and a model-based baseline. Under hardware imperfections in the transmitter ULA, both learning methods outperform the model-based baseline since the assumed model differs from reality. In addition, the model-driven learning approach outperforms neural-network-based learning under complexity constraints and shows better generalization behavior for testing scenarios that are not seen during training. In future works, complexity reduction can be carried out applying pruning [33] techniques to the neural networks. In addition, the sample complexity of the proposed approach could be optimized, for example by introducing physically motivated constraints on the weight matrix $\mathbf{A}$, as in [26]. Moreover, the time complexity of training could potentially be reduced using hard thresholding that produces sparse activations in the network, as in [34].

Acknowledgment

The authors gratefully acknowledge the feedback from Juliano Pinto and Lennart Svensson.

References

[1] A. R. Chiriyath *et al.*, "Radar-communications convergence: Coexistence, cooperation, and co-design," *IEEE Trans. Cogn. Commun. Netw.*, vol. 3, no. 1, pp. 1–12, Feb. 2017.

[2] D. K. P. Tan *et al.*, "Integrated sensing and communication in 6G: Motivations, use cases, requirements, challenges and future directions," in *Proc. Int. Symp. Joint Commun. & Sens.* IEEE, Mar. 2021, pp. 1–6.

[3] H. Wymeersch *et al.*, "Integration of communication and sensing in 6G: a joint industrial and academic perspective," *IEEE PIMRC Workhops*, Sept. 2021.

[4] F. Lampel *et al.*, "A performance enhancement technique for a joint FMCW RADCOM system," in *IEEE Eur. Radar Conf. (EuRAD)*, Oct. 2019, pp. 169–172.

[5] A. Lazaro *et al.*, "Car2car communication using a modulated backscatter and automotive FMCW radar," *Sensors*, vol. 21, no. 11, p. 3656, May 2021.

[6] F. Liu *et al.*, "Integrated sensing and communications: Towards dual-functional wireless networks for 6G and beyond," *IEEE J. Sel. Areas Commun.*, Mar. 2022.

[7] J. A. Zhang *et al.*, "Enabling joint communication and radar sensing in mobile networks—a survey," *IEEE Commun. Surv. & Tut.*, vol. 24, no. 1, pp. 306–345, Oct. 2021.

[8] U. Demirhan *et al.*, "Integrated sensing and communication for 6G: Ten key machine learning roles," *arXiv preprint arXiv:2208.02157*, 2022.

[9] S. Shao *et al.*, "Machine learning-assisted sensing techniques for integrated communications and sensing in WLANs: Current status and future directions," *Prog. Electromagn. Res.*, vol. 175, pp. 45–79, 2022.

[10] Y. Chen *et al.*, "Joint initial access and localization in millimeter wave vehicular networks: a hybrid model/data driven approach," *arXiv preprint arXiv:2204.01510*, 2022.

[11] Y. Wu *et al.*, "Sensing integrated DFT-spread OFDM waveform and deep learning-powered receiver design for terahertz integrated sensing and communication systems," *arXiv preprint arXiv:2109.14918*, 2021.

[12] J. Mu *et al.*, "Integrated sensing and communication-enabled predictive beamforming with deep learning in vehicular networks," *IEEE Commun. Lett.*, vol. 25, no. 10, pp. 3301–3304, Oct. 2021.

[13] C. Liu *et al.*, "Predictive beamforming for integrated sensing and communication in vehicular networks: A deep learning approach," *arXiv preprint arXiv:2202.03811*, 2022.

[14] ——, "Learning-based predictive beamforming for integrated sensing and communication in vehicular networks," *IEEE J. Sel. Areas Comm.*, vol. 40, no. 8, pp. 2317–2334, Jun. 2022.

[15] J. M. Mateos-Ramos *et al.*, "End-to-end learning for integrated sensing and communication," in *IEEE Int. Conf. Commun.*, May 2022, pp. 1942–1947.

[16] J. Liu *et al.*, "A transformer-based signal denoising network for AoA estimation in NLoS environments," *IEEE Commun. Lett.*, Jun. 2022.

[17] T. O'Shea *et al.*, "An Introduction to Deep Learning for the Physical Layer," *IEEE Trans. Cogn. Commun. Netw.*, vol. 3, no. 4, pp. 563–575, dec 2017.

[18] N. Shlezinger *et al.*, "Model-based deep learning," *IEEE Trans. Signal Process.*, Dec. 2020.

[19] ——, "Model-based machine learning for communications," *arXiv preprint arXiv:2101.04726*, 2021.

[20] H. He *et al.*, "Model-driven deep learning for physical layer communications," *IEEE Wireless Commun.*, vol. 26, no. 5, pp. 77–83, Oct. 2019.

[21] K. Gregor *et al.*, "Learning fast approximations of sparse coding," in *Int. Conf. Mach. Learn.* Omnipress, Jun. 2010, pp. 399–406.

[22] J. R. Hershey *et al.*, "Deep unfolding: Model-based inspiration of novel deep architectures," *arXiv preprint arXiv:1409.2574*, 2014.

[23] A. Balatsoukas-Stimming *et al.*, "Deep unfolding for communications systems: A survey and some new directions," in *IEEE Int. Workshop on Signal Process. Syst. (SiPS)*. IEEE, Oct. 2019.

[24] T. Yassine *et al.*, "mpNet: variable depth unfolded neural network for massive MIMO channel estimation," *IEEE Trans. Wireless Commun.*, 2022.

[25] S. Mallat *et al.*, "Matching pursuits with time-frequency dictionaries," *IEEE Trans. Signal Process.*, vol. 41, no. 12, pp. 3397–3415, Dec. 1993.

[26] B. Chatelier *et al.*, "Efficient deep unfolding for SISO-OFDM channel estimation," *arXiv preprint arXiv:2210.06588*, 2022.

[27] A. Alkhateeb *et al.*, "Channel estimation and hybrid precoding for millimeter wave cellular systems," *IEEE J. Sel. Topics Signal Process.*, vol. 8, no. 5, pp. 831–846, Jul. 2014.

[28] J. Tranter *et al.*, "Fast unit-modulus least squares with applications in beamforming," *IEEE Trans. Signal Process.*, vol. 65, no. 11, pp. 2875–2887, Feb. 2017.

[29] J. A. Zhang *et al.*, "Multibeam for joint communication and radar sensing using steerable analog antenna arrays," *IEEE Trans. Veh. Technol.*, vol. 68, no. 1, pp. 671–685, Nov. 2018.

[30] S. Guruacharya *et al.*, "MAP ratio test detector for radar system," *IEEE Trans. Signal Process.*, vol. 69, pp. 573–588, Dec. 2021.

[31] S. Rivetti *et al.*, "Spatial signal design for positioning via end-to-end learning," *arXiv preprint arXiv:2209.12818*, 2022.

[32] D. P. Kingma *et al.*, "Adam: A method for stochastic optimization," *Int. Conf. Learn. Representations*, 2015.

[33] R. Reed, "Pruning algorithms-a survey," *IEEE Trans. Neural Netw.*, vol. 4, no. 5, pp. 740–747, Sep. 1993.

[34] L. Le Magoarou, "Similarity-based prediction for channel mapping and user positioning," *IEEE Commun. Lett.*, vol. 25, no. 5, pp. 1578–1582, Jan. 2021.